Article

Sputtering Power Effects on Growth and Mechanical Properties of Cr₂AlC MAX Phase Coatings

Muhammad Naveed [1], Aleksei Obrosov [1,*], Andrzej Zak [2], Wlodzimierz Dudzinski [2], Alex A. Volinsky [3] and Sabine Weiß [1]

[1] Chair of Physical Metallurgy and Materials Technology, Brandenburg Technical University, Cottbus 03046, Germany; muhammad.naveed@b-tu.de (M.N.); sabine.weiss@b-tu.de (S.W.)

[2] Department of Material Science, Welding and Strength of Material, Wroclaw University of Science and Technology, Wrocław 50370, Poland; andrzej.zak@pwr.edu.pl (A.Z.); wlodzimierz.dudzinski@pwr.edu.pl (W.D.)

[3] University of South Florida, Tampa, FL 33620, USA; volinsky@usf.edu

* Correspondence: aleksei.obrosov@b-tu.de; Tel.: +49-355-694-251

Abstract: Coating growth and mechanical properties of nanolamellar Cr₂AlC coatings at various sputtering power were investigated in the present study. Cr₂AlC coating was deposited on the IN 718 superalloy and (100) Si wafers by DC magnetron sputtering at different sputtering powers. The structure and properties were characterized using X-ray diffraction (XRD), scanning electron microscopy (SEM), transmission electron microscopy (TEM) and nanoindentation. It was found that coatings had columnar structure with nanocrystalline substructure. Deposition rate increased with the sputtering power. XRD results showed the presence of the Cr₂AlC MAX phase, intermetallic AlCr₂ and Cr₇C₃ carbide phases, along with the change in preferential coating growth orientation. TEM observations confirmed the occurrence of these phases, and the SAED patterns demonstrated significant texture of the coatings. Hardness values were measured in the range between 11–14 GPa, showing a slight increase with the sputtering power.

1. Introduction

MAX phase is a group of compounds, which provides a unique combination of metallic and ceramic properties due to the presence of M-A metallic and M-X ceramic bonds. They are nanolamellas with $M_{n+1}AX_n$ (*n* is 1, 2, or 3) chemical formula, where M is an early transition metal, A is an A-group element from the periodic table and X is either carbon or nitrogen [1]. These compounds are known for their low density [1], high stiffness [2,3], superior thermal shock resistance [1,4], damage tolerance [5,6], self-healing behavior [7,8], significant electrical conductivity [4,9], and erosion [10], oxidation [11–16] and hot corrosion resistance [6,17]. Moreover, $M_{n+1}AX_n$ phases have been identified as promising candidates for hydrogen storage applications [18] along with other materials [19,20].

Reports on deposition of the MAX phases as thin films using chemical vapor deposition (CVD) [21] and physical vapor deposition (PVD) [2,22] methods can be found in the literature. Palmquist et al. [23] were the first to deposit the MAX-phase thin coating (Ti₃SiC₂) by physical vapor deposition. Since then, more than 70 compounds have been fabricated through physical vapor deposition and other methods [22,24]. In recent years, ternary carbide Cr₂AlC has attracted much attention because of its excellent high-temperature oxidation and hot corrosion resistance [14,25–27], due to preferential formation of continuous protective Al₂O₃ oxide at high temperatures [15]. Moreover, a small difference

in thermal expansion coefficients between Cr_2AlC and Ni-based alloys makes them along with $Cr_2(Al_x,Ge_{1-x})C$, potential protective film candidates at high temperature [28,29].

Cr_2AlC films can be produced either by sputtering from elemental targets [30–32] or compound targets [10,33]. Literature indicates advantages of lower deposition temperatures for Cr_2AlC [33] in contrast to other MAX phase coatings, like Ti_2AlC and Ti_3AlC_2 [34], which is promising for deposition on heat-sensitive substrates, such as steel. Coating growth depends on a number of process parameters, including substrate bias, deposition temperature, chamber pressure, etc. Sputtering power as a process parameter influences the coating growth, electric resistance, surface roughness [35], mechanical and tribological properties [36]. Past research proved that high metal ionization results from increased sputtering power, eventually affecting coating growth. Extremely high sputtering power could also lead to increased energy of the incoming metal ions, leading to erosion of the already deposited film [37]. Hence, optimization of the sputtering power can lead to better coating design with control of mechanical and chemical properties. However, the effects of sputtering power on coating growth and mechanical properties of Cr_2AlC coatings have not been systemically studied yet. X-ray diffraction (XRD) was utilized to support the arguments provided for the coating growth. Furthermore, correlations between mechanical properties and sputtering power were discussed.

2. Materials and Methods

Cr_2AlC coatings were deposited using a compound target (Cr 50%, Al 25%, and C 25 at. %, 99.9% purity) on IN 718 superalloy and (100) silicon wafers in direct current magnetron sputtering (DCMS) mode. The coating deposition was performed in a CC800/9 industrial coater from CemeCon AG (Würselen, Germany). Prior to deposition, Inconel 718 substrates were wet mirror polished and then cleaned in acetone. The target size was 88 mm × 500 mm and sputtering was performed in a static mode. The distance between the target and the substrate was set at 70 mm. The coating process consisted of a heating phase, followed by argon etching for cleaning organic/foreign particles from the surface and eventually the coating phase. Further details of the deposition process parameters are given in Table 1.

Table 1. Deposition parameters of the Cr_2AlC coatings.

| Process	Parameter	Value
Heating	Temperature, T	550 °C
	Time, t	1.5 h
Argon Etching	Temperature, T	550 °C
	Bias Voltage, V	−650 V
	Argon Pressure, P_{Ar}	350 mPa
	Time, t	0.5 h
Deposition	Temperature, T	550 °C
	Cathode Power, P	1.5 kW/2.5 kW/3.5 kW/4.5 kW
	Bias Voltage, V	−60 V
	Argon Pressure, P_{Ar}	600 mPa
	Time, t	0.5 h

Scanning electron microscopy (SEM, TESCAN Mira, Prague, Czech Republic) was used to investigate the film growth on (100) Si wafers. IN 718 substrates were used for all other investigations. For a global phase determination, D8 Discover X-ray diffractometer (Bruker AXS, Karlsruhe, Germany) with Cu K_α radiation (λ = 0.1546 nm) with an operating voltage of 40 KV and 40 mA current was used. Grazing incidence X-ray diffraction (GIXRD) method with an incident beam angle of 9°, step width of 0.05°, and a 2θ range between 10° and 70° was used for the measurements. Absorption of the incident beam within the Cr_2AlC coating was calculated by means of the AbsorbDX software (Bruker AXS, Karlsruhe, Germany). Moreover, film growth kinetics was also analyzed

by transmission electron microscopy (TEM). Hitachi H-800 TEM (Hitachi High-Technologies Corp., Tokyo, Japan) was operated at 150 kV accelerating voltage. Software developed in the Electron Microscopy Lab at Wroclaw University of Technology (Wroclaw, Poland) was used for local phase analysis, based on electron diffraction patterns. Nanoindentation tests were performed using the UNAT nanoindenter (ASMEC GmbH, Radeberg, Germany) with a Berkovich indenter tip in order to determine mechanical properties (hardness and elastic modulus) of the coatings. By means of the quasi continuous stiffness method (QCSM), the correlation between mechanical properties and penetration depth was determined. A load of 25 mN guaranteed that the penetration depth did not exceed 1/10th of the coating thickness [38] whereas, the load–displacement curves were analyzed using the Oliver Pharr method [39].

3. Results and Discussion

3.1. Coating Deposition Rate

The deposition rate of the Cr_2AlC coatings using DCMS shows almost linear relationship with the sputtering power. Deposition rate increase of almost 100% can be seen with the sputtering power increase from 1.5 kW to 4.5 kW in Figure 1.
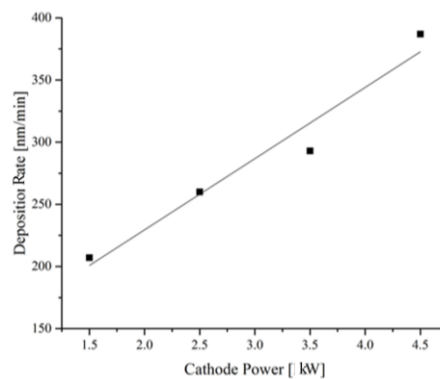

Figure 1. Relationship between the sputtering power and deposition rate of the Cr_2AlC coatings.

This deposition rate increase with the sputtering power could be correlated with increased flux of metal atoms. An increase in Ar ion flux within the coating chamber enhances the probability of ejection of higher number of metal ions from the target. Farooq and Lee [40] found that the maximum chamber pressure shifts from lower towards higher values with the cathode power increase. It was concluded that the sputtering current is a major factor affecting the sputtering yield of a target, which could vary with the type of the target.

3.2. Phase Identification

To avoid reflections from the substrate material, low incident beam angle of 9° was chosen for the measurements. In the measured range (10°–70°) there are two super lattice reflections: (002) and (101), which correspond to ordered Cr_2AlC MAX phase [32,41]. At approximately 13.3°, (002) weak reflection for all coatings was observed, identifying the presence of the MAX phase within the coating [32]. The (101) reflection cannot be clearly recognized, probably due to the coincidence with the (100) reflection [41]. XRD pattern of the film deposited with a cathode power of 1.5 kW reveals the presence of (100/101) and (110) planes (Figure 2), whereas coatings deposited at 2.5 kW and 3.5 kW show (103) preferred orientation growth. At 4.5 kW (100/101) planes preferential growth can be seen again with the disappearance of this (110) peak. A relatively high (110) plane intensity was observed at 1.5 kW compared with 2.5 kW. Further increase of the cathode power to 4.5 kW leads to a complete

disappearance of this peak. This variation of preferred orientation with the sputtering power can be correlated with the accumulation of surface and strain energy during the coating process [42].
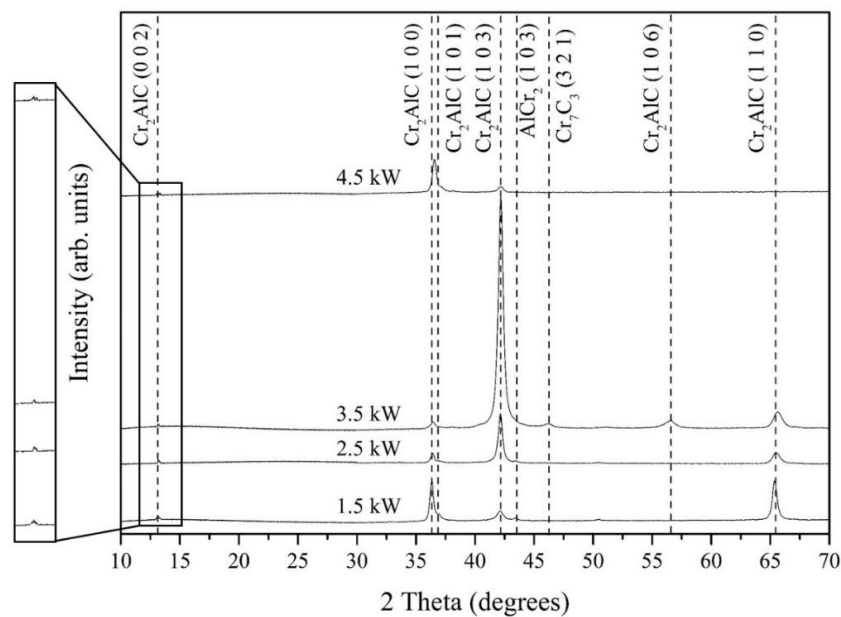
Figure 2. X-ray diffraction (XRD) spectra of Cr_2AlC coatings deposited at various sputtering power.

According to Chawla et al. [42], the surface and interface energies are responsible for controlling the coating preferred orientation. As the thickness of the coatings increases, higher strains appear within the coating, leading to coating growth control through strain energy [43]. A similar theory has been presented by Quaeyhaegegens et al. [44], who reported a change in preferential plane growth of TiN coatings with increased thickness. As reported in the previous section, higher coating thickness has been observed for 4.5 kW compared with 3.5 kW sputtering power for the same deposition time. Therefore, it can be assumed that a critical thickness of the coating was achieved at a sputtering power of 3.5 kW, which supports the coating growth in the (103) direction. After this thickness, the adatoms orient themselves in another preferential orientation due to strain energy, showing (100/101) dominant diffraction peaks at 4.5 kW. Moreover, the presence of intermetallic $AlCr_2$ phase was identified for 1.5 kW and 2.5 kW, whereas Cr_7C_3 phase peak was found only at 3.5 kW. Comparison of all coatings shows that preferential (103) planes grew during the deposition process instead of (110) or (100/101). A dominant (103) diffraction peak has been reported by Zamulaeva et al. [45,46] for the Cr_2AlC coatings deposited on Ti substrates, as well as by Field [47]. In contrast, Li et al. [48] discussed preferential coating growth at (110) planes taking place during deposition on the M38G super alloy. Hence, variations of the substrate, process kinetics, substrate surface energy, etc., can be regarded as influencing parameters affecting the coating growth.

3.3. Coating Microstructure

A columnar structure of the deposited coatings can be seen in Figure 3. The coating deposited at 1.5 kW demonstrates column thickness in the 200–500 nm range in Figure 3a, whereas a corresponding surface morphology can be seen in Figure 3b. The column diameter increases during the deposition at 2.5 kW and the column size can be estimated above 500 nm (Figure 3c). At this sputtering power, a feathery flower-like structure appears on the surface of the coatings in Figure 3d. Up to 2.5 kW sputtering power, the coating columns grew with a certain orientation from the specimen normal with a dense structure. As the sputtering power was increased to 3.5 kW, the density of this flower structure increased on the surface of the coating, but a feathery appearance can still be seen in Figure 3f. Comparatively, porous structure is observed at lower sputtering power in

Figure 3e. Strong renucleation of columns could be noticed during deposition at 4.5 kW (Figure 3e,f). This renucleation of columns can be regarded as density defect, which interrupts local epitaxy of the individual columns and takes place when the ion energy becomes large enough to support continuous coating growth [49]. A shark skin structure can be seen for the coating deposited at 4.5 kW in Figure 3h.
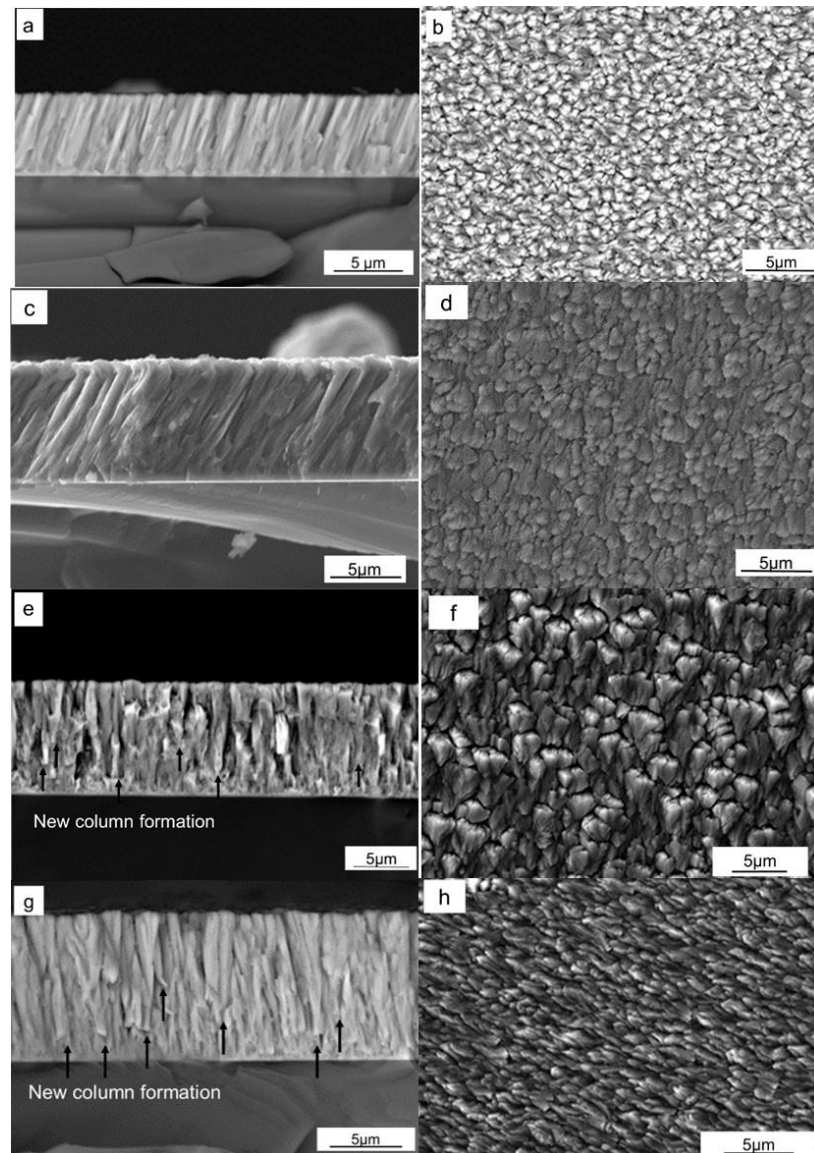
Figure 3. (**a**,**c**,**e**,**g**) Cross-sectional; and (**b**,**d**,**f**,**h**) surface morphology of Cr_2AlC coatings deposited at: (**a**,**b**) 1.5 kW; (**c**,**d**) 2.5 kW; (**e**,**f**) 3.5 kW; and (**g**,**h**) 4.5 kW, respectively.

Cross-sectional TEM images of the Cr_2AlC deposited at 2.5 kW were analyzed to evaluate the coating growth. The coating layer exhibits low porosity columnar structure in Figure 4a with 100–300 nm width range, oriented at $\pm15°$ angle with respect to the substrate normal. Selected area electron diffraction (SAED) images taken from an area near the substrate show the Cr_2AlC phase presence. Discontinuous diffraction rings confirm polycrystalline structure of the coating and presence of a significant texture (Figure 4b). Columns of the Cr_2AlC crystals present the local nanocrystalline structure and show [012] growth direction in Figure 4c,d. Presence of an intermetallic $AlCr_2$ phase can be observed in the top layer of the coating too (Figure 4e). The grains show [112] orientation, which is nearly parallel to the main growth axis of the coating, while the $[1\bar{1}0]$ direction is parallel to the incident electron beam. SAED reveals fuzzy streaks and extra diffraction spots along the [002]

direction in Figure 4f. The reason of these supplementary diffraction spots could be the presence of a super lattice formed in the [002] direction, ordered stacking faults [50] or another long-range atomic plane arrangements. Low intermetallic phase presence is observed only for the coatings deposited at 1.5 and 2.5 kW, showing weak (103) reflections identified by the XRD measurements.
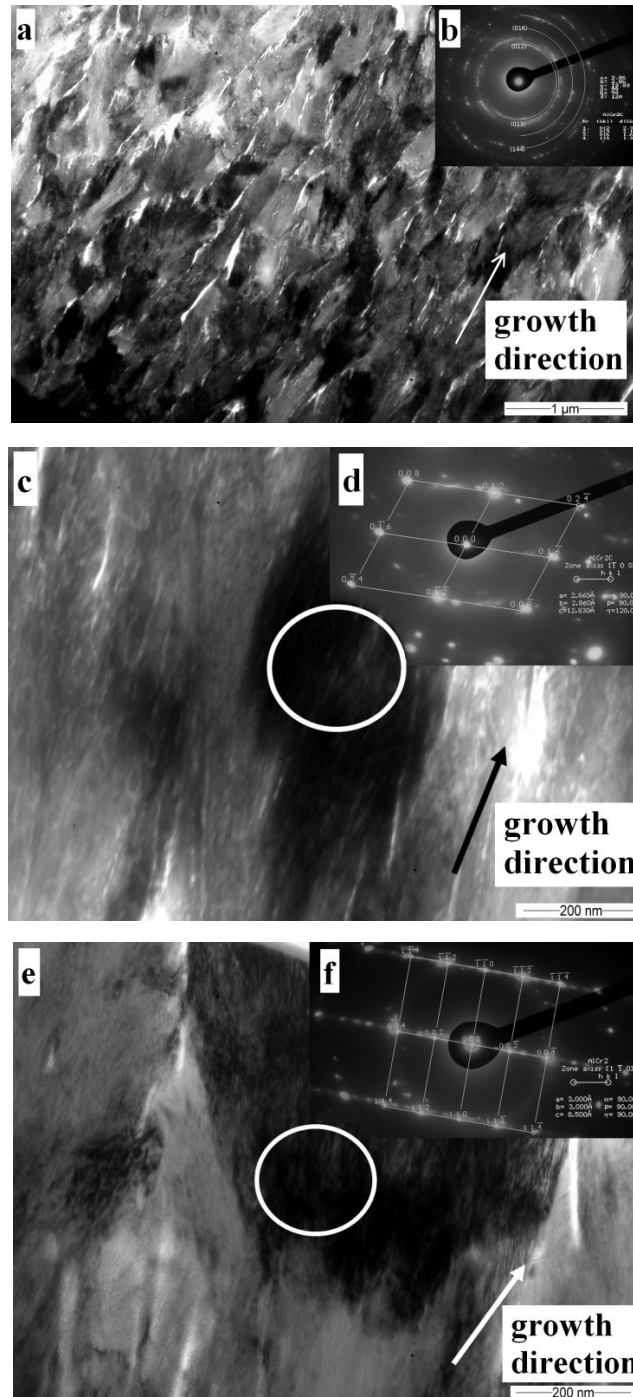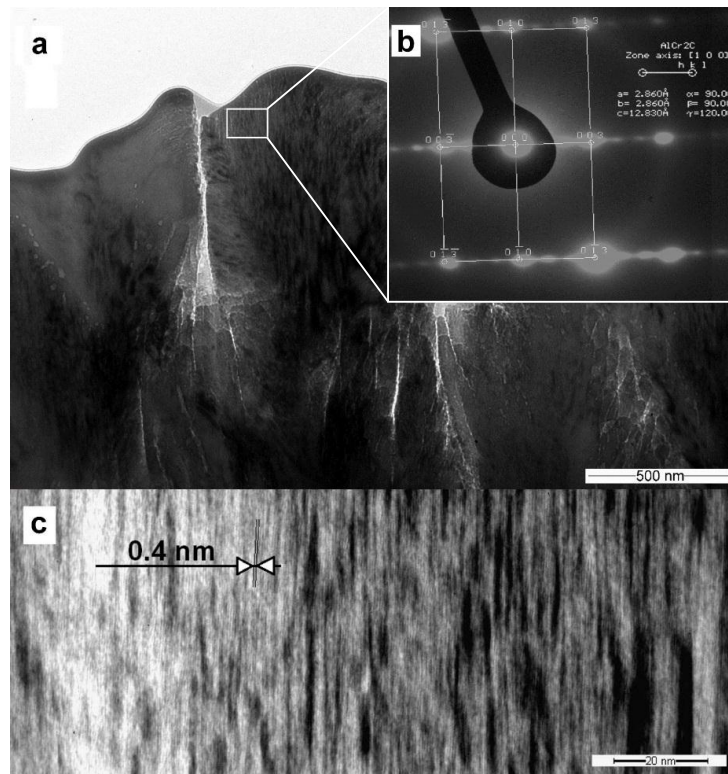

Figure 4. (**a**,**c**,**e**) Bright-field images; and (**b**,**d**,**f**) calculated SAED patterns of Cr$_2$AlC coating deposited at 2.5 kW sputtering power. SAED patterns were taken from the marked areas.

A bright field TEM image of the coating surface can be seen in Figure 5, showing 200 nm wide columns including a 24 nm sub-grain size. Moreover, these columns seem to be densely packed with low porosity. These results are in agreement with the SEM images as shown in Figure 4c,d.
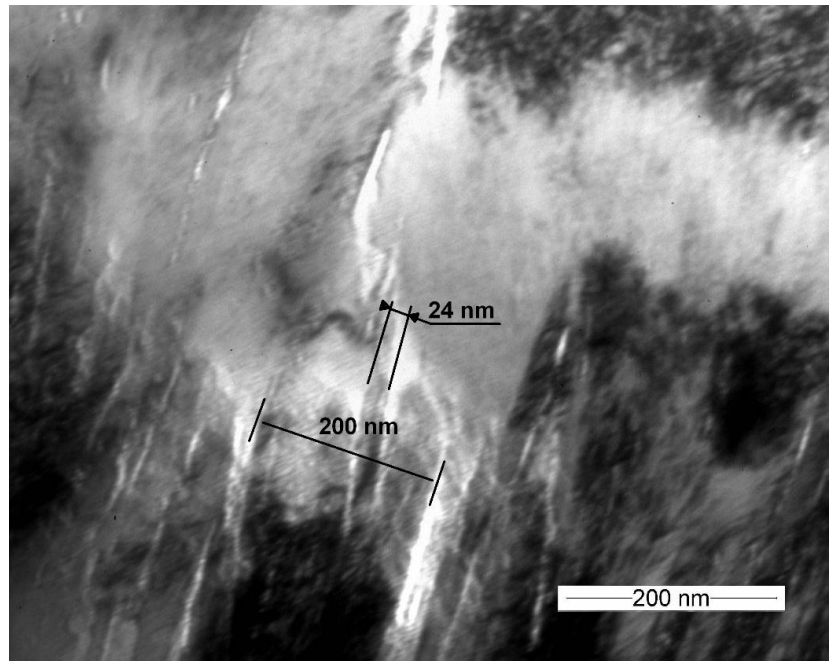
Figure 5. Bright-field image of the Cr$_2$AlC coating deposited at 2.5 kW sputtering power, showing column width and nanoscale subgrains.

Figure 6. (**a**) Bright-field image and (**b**) the corresponding calculated SAED pattern and (**c**) magnification showing (003) lattice image of the Cr$_2$AlC coating deposited at 2.5 kW sputtering power.

Presence of the superlattice structure has also been found for some of the Cr$_2$AlC crystals by TEM analysis in Figure 6a. SAED pattern obtained with an electron beam parallel to the [100] direction,

reveals fuzzy streaks and extra diffraction spots along the [003] direction in Figure 6b. Estimation of the lattice parameters of this Cr_2AlC hexagonal phase shows an interplanar distance of approximately 0.427 nm (Figure 6c). This is contrary to literature, as an interplaner distance of 1.2 nm was investigated for Cr_2AlC lattice structure [22] which cannot be observed in our measurements due to the twinning effect [22].

3.4. Mechanical Properties

Hardness (*H*) and elastic modulus (*E*) of the Cr_2AlC coatings are listed in Table 2. These two properties are selected for the present study as they describe the behavior of wear resisting materials. High hardness represents resistance against indenter penetration during plastic deformation whereas high E-Modulus leads to distribution of load on a large area [51]. In the current study, high hardness values of the deposited Cr_2AlC coatings are measured as compared to literature [52,53]. Hardness and elastic modulus values of the deposited Cr_2AlC coatings could be interpreted in terms of the sputtering power change. Elastic strain to failure (H/E), defined as significant factor in wear control [54], was calculated as an average value of 0.04 for the coatings. Plastic strain to failure (H^3/E^2) ratio, which defines the resistance of the material against plastic deformation [55], does not show large variations. In comparison, high plastic strain to plastic deformation of DLC [56] and TiAlN coatings [57] makes Cr_2AlC inappropriate for wear applications.

Table 2. Influence of the sputtering power on mechanical properties of the Cr_2AlC coatings.

Cathode Power, kW	Hardness, GPa	Elastic modulus, GPa	H/E	H^3/E^2, GPa
1.5	11.5 ± 2.8	288.6 ± 84.7	0.03 ± 0.02	0.018 ± 0.02
2.5	12.1 ± 4.7	287.2 ± 88.8	0.04 ± 0.02	0.021 ± 0.03
3.5	13.9 ± 4.6	289.2 ± 111	0.04 ± 0.03	0.032 ± 0.05
4.5	12.3 ± 2.0	281.1 ± 54.5	0.04 ± 0.01	0.023 ± 0.02

A slight increase of hardness was observed with increasing sputtering power together with a constant elastic modulus. Thus, an increase in H/E and H^3/E^2 was calculated. At the sputtering power of 4.5 kW, a slight decrease in hardness was noticed, which could be related to the carbide formation within the coating. Ying et al. [52] found that different carbide phases and the amount of a particular carbide phase influence the mechanical properties (hardness and elastic modulus) of the coatings. They reported that a lower amount of the Cr_7C_3 phase (0%–14%) shows low hardness (4.7–5.5 GPa), whereas an increase above 17% resulted in values above 6 GPa. Similarly, hardness of the Cr_3C_2 carbide phase was reported between 15.1–18.9 GPa, which was correlated with the grain size of the corresponding phase [58]. Therefore, quantification of the phases through the Rietveld refinement would be a preferable method for correlating phases and mechanical properties. This approach will be discussed in further publications.

4. Conclusions

Columnar structure has been determined for all coatings with the presence of Cr_2AlC MAX as the main phase along with traces of $AlCr_2$ intermetallic as well as carbide phases. The Cr_2AlC films observed by TEM showed nanocrystalline substructure with a column thickness in the 100–200 nm range along with high texture of the coatings. Moreover, an increase in coating growth occurred with the increase in sputtering power and a change in preferential coating growth orientation took place. Hardness and elastic modulus values indicate that these films cannot be introduced in aggressive wear applications due to low hardness. However, these coatings still have the capability to be used in high temperature and low friction applications due to their self-healing capabilities.

Author Contributions: Muhammad Naveed carried out the deposition process, analyzed the results and prepared the manuscript. Aleksei Obrosov was responsible for carrying out detailed XRD and TEM analysis, was involved in manuscript writing along with the correction of the manuscript during the review phase. Andrzej Zak and Wlodzimierz Dudzinski provided the TEM observations and analyzed the SAED data. Alex A. Volinsky and Sabine Weiß did the revision and direction of the work.

Conflicts of Interest: The authors declare no conflict of interest.

References

1. Barsoum, M.W. The MN + 1AXN phases: A new class of solids: Thermodynamically stable nanolaminates. *Prog. Solid State Chem.* **2000**, *28*, 201–281. [CrossRef]

2. Schneider, J.M.; Sigumonrong, D.P.; Music, D.; Walter, C.; Emmerlich, J.; Iskandar, R.; Mayer, J. Elastic properties of Cr_2AlC thin films probed by nanoindentation and ab initio molecular dynamics. *Scr. Mater.* **2007**, *57*, 1137–1140. [CrossRef]

3. Hettinger, J.D.; Lofland, S.E.; Finkel, P.; Meehan, T.; Palma, J.; Harrell, K.; Gupta, S.; Ganguly, A.; El-Raghy, T.; Barsoum, M.W. Electrical transport, thermal transport, and elastic properties of M_2AlC (M = Ti, Cr, Nb and V). *Phys. Rev. B* **2005**, *72*, 115120. [CrossRef]

4. Barsoum, M.W.; El-Raghy, T. Synthesis and Characterization of a Remarkable Ceramic: Ti_3SiC_2. *J. Am. Ceram. Soc.* **1996**, *79*, 1953–1956. [CrossRef]

5. Tzenov, N.V.; Barsoum, M.W. Synthesis and Characterization of Ti_3AlC_2. *J. Am. Ceram. Soc.* **2000**, *83*, 825–832. [CrossRef]

6. Abdulkadhim, A.; Baben, M.; Takahashi, T.; Schnabel, V.; Hans, M.; Polzer, C.; Polcik, P.; Schneider, J.M. Crystallization kinetics of amorphous Cr_2AlC thin films. *Surf. Coat. Technol.* **2011**, *206*, 599–603. [CrossRef]

7. Song, G.M.; Pei, Y.T.; Sloof, W.G.; Li, S.B.; de Hosson, J.T.M.; van der Zwaag, S. Oxidation-induced crack healing in Ti_3AlC_2 ceramics. *Scr. Mater.* **2008**, *58*, 13–16. [CrossRef]

8. Yang, H.J.; Pei, Y.T.; Rao, J.C.; de Hosson, J.T.M.; Li, S.B.; Song, G.M. High temperature healing of Ti_2AlC: On the origin of inhomogeneous oxide scale. *Scr. Mater.* **2011**, *65*, 135–138. [CrossRef]

9. Wang, P.; Mei, B.; Hong, X.; Zhou, W. Synthesis of Ti_2AlC by hot pressing and its mechanical and electrical properties. *Trans. Nonferr. Met. Soc. China* **2007**, *17*, 1001–1004. [CrossRef]

10. Naveed, M.; Renteria, A.F.; Nebel, D.; Weiß, S. Study of high velocity solid particle erosion behaviour of Ti_2AlC MAX phase coatings. *Wear* **2015**, *342–343*, 391–397. [CrossRef]

11. Hajas, D.E.; Baben, M.; Hallstedt, B.; Iskandar, R.; Mayer, J.; Schneider, J.M. Oxidation of Cr_2AlC coatings in the temperature range of 1230 to 1410 °C. *Surf. Coat. Technol.* **2011**, *206*, 591–598. [CrossRef]

12. Wang, X.H.; Zhou, Y.C. Intermediate-temperature oxidation behavior of Ti_2AlC in air. *J. Mater. Res.* **2002**, *17*, 2974–2981. [CrossRef]

13. Wang, X.H.; Zhou, Y.C. Oxidation behavior of Ti_3AlC_2 at 1000–1400 °C in air. *Corros. Sci.* **2003**, *45*, 891–907. [CrossRef]

14. Tian, W.; Wang, P.; Kan, Y.; Zhang, G. Oxidation behavior of Cr_2AlC ceramics at 1100 and 1250 °C. *J. Mater. Sci.* **2008**, *43*, 2785–2791. [CrossRef]

15. Baben, M.; Shang, L.; Emmerlich, J.; Schneider, J.M. Oxygen incorporation in M_2AlC (M = Ti, V, Cr). *Acta Mater.* **2012**, *60*, 4810–4818. [CrossRef]

16. Li, J.J.; Qian, Y.H.; Niu, D.; Zhang, M.M.; Liu, Z.M.; Li, M.S. Phase formation and microstructure evolution of arc ion deposited Cr_2AlC coating after heat treatment. *Appl. Surf. Sci.* **2012**, *263*, 457–464. [CrossRef]

17. Lin, Z.J.; Li, M.S.; Wang, J.Y.; Zhou, Y.C. High-temperature oxidation and hot corrosion of Cr_2AlC. *Acta Mater.* **2007**, *55*, 6182–6191. [CrossRef]

18. Ding, H.; Glandut, N.; Fan, X.; Liu, Q.; Shi, Y.; Jie, J. First-principles study of hydrogen incorporation into the MAX phase Ti_3AlC_2. *Int. J. Hydrog. Energy* **2016**, *41*, 6387–6393. [CrossRef]

19. Kashkarov, E.B.; Nikitenkov, N.N.; Sutygina, A.N.; Syrtanov, M.S.; Vilkhivskaya, O.V.; Pryamushko, T.S.; Kudiiarov, V.N.; Volesky, L. Effect of titanium ion implantation and deposition on hydrogenation behavior of Zr-1Nb alloy. *Surf. Coat. Technol.* **2016**. [CrossRef]

20. Kashkarov, E.B.; Nikitenkov, N.N.; Syrtanov, M.S.; Sutygina, A.N.; Shulepov, I.A.; Lider, A.M. Influence of plasma immersion titanium implantation on hydrogenation and mechanical properties of Zr-2.5Nb. *Appl. Surf. Sci.* **2016**, *370*, 142–148. [CrossRef]

21. Fakih, H.; Jacques, S.; Berthet, M.P.; Bosselet, F.; Dezellus, O.; Viala, J.C. The growth of Ti_3SiC_2 coatings onto SiC by reactive chemical vapor deposition using H_2 and $TiCl_4$. *Surf. Coat. Technol.* **2006**, *201*, 3748–3755. [CrossRef]

22. Eklund, P.; Beckers, M.; Jansson, U.; Högberg, H.; Hultman, L. The Mn + 1AXn phases: Materials science and thin-film processing. *Thin Solid Films* **2010**, *518*, 1851–1878. [CrossRef]

23. Palmquist, J.-P.; Jansson, U.; Seppänen, T.; Persson, P.O.A.; Birch, J.; Hultman, L.; Isberg, P. Magnetron sputtered epitaxial single-phase Ti_3SiC_2 thin films. *Appl. Phys. Lett.* **2002**, *81*, 835–837. [CrossRef]

24. Barsoum, M.W.; Radovic, M. Elastic and Mechanical Properties of the MAX Phases. *Annu. Rev. Mater. Res.* **2011**, *41*, 195–227. [CrossRef]

25. Lee, D.B.; Nguyen, T.D. Cyclic oxidation of Cr_2AlC between 1000 and 1300 °C in air. *J. Alloy. Compd.* **2008**, *464*, 434–439. [CrossRef]

26. Wang, Q.M.; Renteria, A.F.; Schroeter, O.; Mykhaylonka, R.; Leyens, C.; Garkas, W.; Baben, M. Fabrication and oxidation behavior of Cr_2AlC coating on Ti6242 alloy. *Surf. Coat. Technol.* **2010**, *204*, 2343–2352. [CrossRef]

27. Smialek, J.L.; Garg, A. Interfacial reactions of a MAX phase/superalloy hybrid. *Surf. Interface Anal.* **2015**, *47*, 844–853. [CrossRef]

28. Li, J.J.; Li, M.S.; Xiang, H.M.; Lu, X.P.; Zhou, Y.C. Short-term oxidation resistance and degradation of Cr_2AlC coating on M38G superalloy at 900–1100 °C. *Corros. Sci.* **2011**, *53*, 3813–3820. [CrossRef]

29. Cabioch, T.; Eklund, P.; Mauchamp, V.; Jaouen, M.; Barsoum, M.W. Tailoring of the thermal expansion of $Cr_2(Al_x,Ge_{1-x})C$ phases. *J. Eur. Ceram. Soc.* **2013**, *33*, 897–904. [CrossRef]

30. Mertens, R.; Sun, Z.; Music, D.; Schneider, J.M. Effect of the Composition on the Structure of Cr-Al-C Investigated by Combinatorial Thin Film Synthesis and ab Initio Calculations. *Adv. Eng. Mater.* **2004**, *6*, 903–907. [CrossRef]

31. Schneider, J.M.; Sun, Z.; Mertens, R.; Uestel, F.; Ahuja, R. Ab initio calculations and experimental determination of the structure of Cr_2AlC. *Solid State Commun.* **2004**, *130*, 445–449. [CrossRef]

32. Grieseler, R.; Hähnlein, B.; Stubenrauch, M.; Kups, T.; Wilke, M.; Hopfeld, M.; Pezoldt, J.; Schaaf, P. Nanostructured plasma etched, magnetron sputtered nanolaminar Cr_2AlC MAX phase thin films. *Appl. Surf. Sci.* **2014**, *292*, 997–1001. [CrossRef]

33. Walter, C.; Sigumonrong, D.P.; El-Raghy, T.; Schneider, J.M. Towards large area deposition of Cr_2AlC on steel. *Thin Solid Films* **2006**, *515*, 389–393. [CrossRef]

34. Wilhelmsson, O.; Palmquist, J.-P.; Nyberg, T.; Jansson, U. Deposition of Ti_2AlC and Ti_3AlC_2 epitaxial films by magnetron sputtering. *Appl. Phys. Lett.* **2004**, *85*, 1066–1068. [CrossRef]

35. Le, M.-T.; Sohn, Y.-U.; Lim, J.-S.; Choi, G.-S. Effect of Sputtering Power on the Nucleation and Growth of Cu Films Deposited by Magnetron Sputtering. *Mater. Trans.* **2010**, *51*, 116–120. [CrossRef]

36. Wang, P.; Takeno, T.; Fontaine, J.; Aono, M.; Adachi, K.; Miki, H.; Takagi, T. Effects of substrate bias voltage and target sputtering power on the structural and tribological properties of carbon nitride coatings. *Mater. Chem. Phys.* **2014**, *145*, 434–440. [CrossRef]

37. Rossnagel, S.M.; Hopwood, J. Magnetron sputter deposition with high levels of metal ionization. *Appl. Phys. Lett.* **1993**, *63*, 3285–3287. [CrossRef]

38. Naveed, M.; Obrosov, A.; Weiß, S. Investigation of the Wear Resistance Properties of Cr/CrN Multilayer Coatings against Sand Erosion. *Conf. Pap. Sci.* **2015**, *2015*, 9. [CrossRef]

39. Oliver, W.C.; Pharr, G.M. An improved technique for determining hardness and elastic modulus using load and displacement sensing indentation experiments. *J. Mater. Res.* **1992**, *7*, 1564–1583. [CrossRef]

40. Farooq, M.; Lee, Z.H. Optimization of the sputtering process for depositing composite thin films. *J. Korean Phys. Soc.* **2002**, *40*, 511–515.

41. Berger, O.; Leyens, C.; Heinze, S.; Boucher, R.; Ruhnow, M. Characterization of Cr–Al–C and Cr–Al–C–Y films synthesized by High Power Impulse Magnetron Sputtering at a low deposition temperature. *Thin Solid Films* **2015**, *580*, 6–11. [CrossRef]

42. Chawla, V.; Jayaganthan, R.; Chawla, A.K.; Chandra, R. Microstructural characterizations of magnetron sputtered Ti films on glass substrate. *J. Mater. Process. Technol.* **2009**, *209*, 3444–3451. [CrossRef]

43. Thompson, C.V. Structure evolution during processing of polycrystalline films. *Annu. Rev. Mater. Sci.* **2000**, *30*, 159–190. [CrossRef]

44. Quaeyhaegens, C.; Knuyt, G.; D'Haen, J.; Stals, L.S. Experimental study of the growth evolution from random towards a (111) preferential orientation of PVD TiN coatings. *Thin Solid Films* **1995**, *258*, 170–173. [CrossRef]

45. Zamulaeva, E.I.; Levashov, E.A.; Sviridova, T.A.; Shvyndina, N.V.; Petrzhik, M.I. Pulsed electrospark deposition of MAX phase Cr_2AlC based coatings on titanium alloy. *Surf. Coat. Technol.* **2013**, *235*, 454–460. [CrossRef]

46. Zamulaeva, E.I.; Levashov, E.A.; Skryleva, E.A.; Sviridova, T.A.; Kiryukhantsev-Korneev, P.V. Conditions for formation of MAX phase Cr_2AlC in electrospark coatings deposited onto titanium alloy. *Surf. Coat. Technol.* **2016**, *298*, 15–23. [CrossRef]

47. Field, M.R.; Carlsson, P.; Eklund, P.; Partridge, J.G.; McCulloch, D.G.; McKenzie, D.R.; Bilek, M.M.M. A combinatorial comparison of DC and high power impulse magnetron sputtered Cr_2AlC. *Surf. Coat. Technol.* **2014**, *259*, 746–750. [CrossRef]

48. Li, J.J.; Hu, L.F.; Li, F.Z.; Li, M.S.; Zhou, Y.C. Variation of microstructure and composition of the Cr_2AlC coating prepared by sputtering at 370 and 500 °C. *Surf. Coat. Technol.* **2010**, *204*, 3838–3845. [CrossRef]

49. Petrov, I.; Barna, P.B.; Hultman, L.; Greene, J.E. Microstructural evolution during film growth. *J. Vac. Sci. Technol. A* **2003**, *21*, S117–S128. [CrossRef]

50. Dudzinski, W.; Morniroli, J.P.; Gantois, M. Stacking faults in chromium, iron and vanadium mixed carbides of the type M7C3. *J. Mater. Sci.* **1980**, *15*, 1387–1401. [CrossRef]

51. Kim, G.S.; Lee, S.Y.; Hahn, J.H.; Lee, S.Y. Synthesis of CrN/AlN superlattice coatings using closed-field unbalanced magnetron sputtering process. *Surf. Coat. Technol.* **2003**, *171*, 91–95. [CrossRef]

52. Ying, G.; He, X.; Li, M.; Du, S.; Han, W.; He, F. Effect of Cr_7C_3 on the mechanical, thermal, and electrical properties of Cr_2AlC. *J. Alloy. Compd.* **2011**, *509*, 8022–8027. [CrossRef]

53. Hopfeld, M.; Grieseler, M.; Vogel, A.; Romanus, H.; Schaaf, P. Tribological behavior of selected Mn + 1AXn phase thin films on silicon substrates. *Surf. Coat. Technol.* **2014**, *257*, 286–294. [CrossRef]

54. Leyland, A.; Matthews, A. On the significance of the H/E ratio in wear control: A nanocomposite coating approach to optimised tribological behaviour. *Wear* **2000**, *246*, 1–11. [CrossRef]

55. Musil, J. Hard and superhard nanocomposite coatings. *Surf. Coat. Technol.* **2000**, *125*, 322–330. [CrossRef]

56. Voevodin, A.A.; Zabinski, J.S. Superhard, functionally gradient, nanolayered and nanocomposite diamond-like carbon coatings for wear protection. *Diam. Relat. Mater.* **1998**, *7*, 463–467. [CrossRef]

57. Musil, J.; Hrubý, H. Superhard nanocomposite $Ti_{1-x}Al_xN$ films prepared by magnetron sputtering. *Thin Solid Films* **2000**, *365*, 104–109. [CrossRef]

58. Hirota, K.; Mitani, K.; Yoshinaka, M.; Yamaguchi, O. Simultaneous synthesis and consolidation of chromium carbides (Cr_3C_2, Cr_7C_3 and $Cr_{23}C_6$) by pulsed electric-current pressure sintering. *Mater. Sci. Eng. A* **2005**, *399*, 154–160. [CrossRef]